Supplementary Information

Dynamics of Hydrogen Nanobubbles in KLH Protein Solution Studied with In-Situ Wet-TEM

Tsu-Wei Huang,[a] *Shih-Yi Liu,*[a] *Yun-Ju Chuang,*[b] *Hsin-Yi Hsieh,*[c] *Chun-Ying Tsai,*[a] *Wei-Jung Wu,*[a] *Cheng-Ting Tsai,*[d] *Utkur Mirsaidov,*[e] *Paul Matsudaira,*[f] *Chia-Shen Chang,*[g] *Fan-Gang Tseng*[*a,c,h] *and Fu-Rong Chen*[*a]

† The first two authors contributed equally to this work.

[a]Department of Engineering and System Science, National Tsing Hua University, Hsinchu 30013, Taiwan

[b]Department of Biomedical Engineering, Ming Chuan University, Taoyuan 33345, Taiwan

[c]Institute of NanoEngineering and MicroSystems, National Tsing Hua University, Hsinchu 30013, Taiwan

[d]Department of Materials Engineering, National Chung Hsing University, Taichung 402, Taiwan

[e]Mechanobiology Institute, National University of Singapore, Singapore 119077

[f]Department of Biological Sciences, National University of Singapore, Singapore 119077

[g]Institute of Physics, Academic Sinica, Nankang, Taipei 11529, Taiwan

[h]Division of Mechanics, Research Center for Applied Science, Academia Sinica, Nankang, Taipei 11529, Taiwan

[*] Corresponding author: Fu-Rong Chen, No. 101, Section 2, Kuang-Fu Road, Hsinchu 30013, Taiwan, Tel: +886-3-5762249; Fax: +886-3-5734066; E-mail: frchen@ess.nthu.edu.tw

[*] Corresponding author: Fan-Gang Tseng, No. 101, Section 2, Kuang-Fu Road, Hsinchu 30013, Taiwan, Tel: +886-3-5715131 #34270; Fax: +886-3-5720724; E-mail: fangang@ess.nthu.edu.tw

Comparison of electron-beam illumination on the dried and aqueous KLH protein

Fig. S1(a) is a TEM image of atmospheric dried KLH protein on the silicon nitride membrane. The morphology of aggraded KLH protein is not clear due to the weak contrast of light element (no staining was used in all the experiments). Gold nanoparticles (darker contrast) are used to find the position of the focus plane for TEM operation. Even under a high-dose illumination (fluence rate: 5000 $e^-/Å^2 \cdot s$, irradiation time: 10 min), no bubbling was observed on the fully dehydrated sediment composited of the KLH aggregates and the salt residue from PBS solution.

Fig. S1(b) shows the aggregation of hydrated KLH protein suspended in the liquid. The low fluence rate of 24.9 $e^-/Å^2 \cdot s$ was adopted to avoid the electron-beam induced bubbling, and the picture was made of 20-images averaging to enhance the signal to noise ratio (exposure time: 0.8 s, interval time: 7 s). Although the giant KLH aggregates (molecular weight of 0.5−13 million Daltons) is poor in water solubility, the subunit isoforms (KLH1 and KLH2) with smaller size (~3.7 nm in diameter, ~4 nm in height) still have a better dispersion in solution.

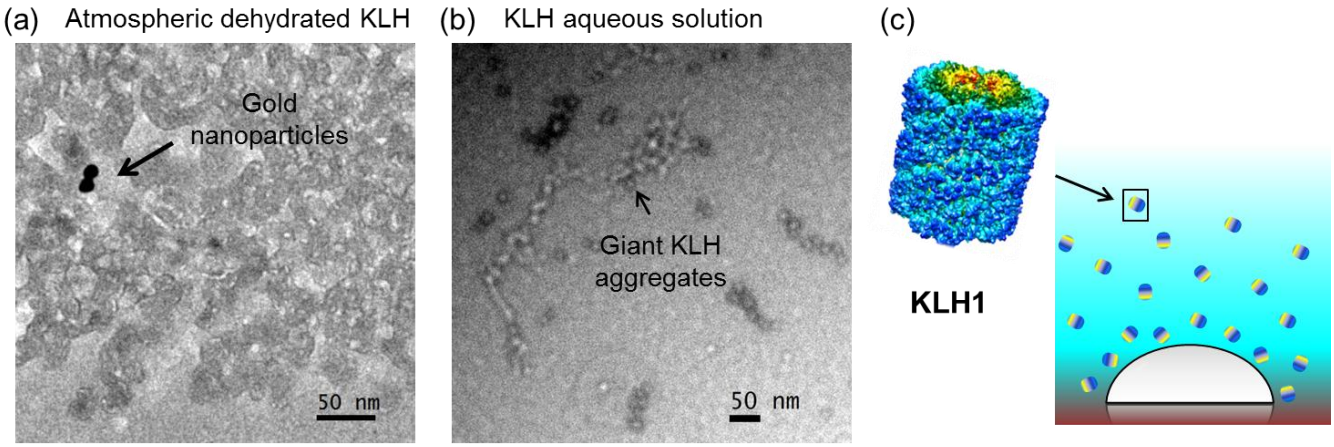

Fig. S1. TEM images of KLH protein aggregates. (a) A TEM image of dehydrated KLH protein. (b) A TEM image of KLH protein suspension sealed in SAW cell. (c) The molecular model (from EMDB 1569) is the subunit of protein molecular (KLH1) with smaller size[1].

A video of dynamic evolution of growing nanobubbles

See Movie S1 at http://oz.nthu.edu.tw/~d9511814/supporting/MOVIES1.avi . The half side presents a sequence of color-coded TEM images of a cluster of growing NBs. The right-half side presents the dynamic tracking and analysis of NB diameters.

Temperature rising induced by electron-beam heating

To verify the mechanism of bubbling in protein solution, the possibility of nucleate boiling by electron-beam heating are estimated. Base on the radiation damage hypothesis purposed by Egerton,[2] the eqn (S1) describes the steady-state energy balance of heat generation from inelastic electron collision and the heat loss due to conduction and radiation. We can use this equation to calculate the temperature rising ($\Delta T = T - T_0$) resulted from the electron-beam interaction with the SAW cell sample. In general, the thickness of liquid sample is 50 μm, and the total thickness of two silicon nitride membranes is 100 nm. Other dimensions are schematic drawing in Fig. S2(a) (not to scale).

$$I\left\langle E(eV)\right\rangle\left(\frac{t}{\lambda}\right)=\frac{4\pi\kappa t\left(T-T_0\right)}{0.58+2\ln(\frac{2R_0}{d})}+\pi\frac{x^2}{2}\varepsilon\sigma\left(T^4-T_0^4\right) \qquad \text{(S1)}$$

$$\lambda_i = 106F\frac{\left(\frac{E_0}{\langle E\rangle}\right)}{\ln\left(2\beta\frac{E_0}{\langle E\rangle}\right)} \qquad \text{(S1)}$$

$$F=\frac{\left(1+\frac{E_0}{1022}\right)}{\left(1+\frac{E_0}{511}\right)^2} \qquad \text{(S2)}$$

$$\langle E\rangle = 7.6Z^{0.36} \qquad \text{(S3)}$$

I is the incident beam current (typical in the range of 10 pA – 10 nA), $\langle E \rangle$ is the average energy loss per inelastic collision, e is the electronic charge, t is the thickness of material, λ_i is the inelastic electron mean free path. Both $\langle E \rangle$ and λ_i are dependent on the mean atomic number (Z) of material composition and could be calculated by the eqn (S2)-(S4) (corresponding results are shown in Table. S1).[3] E_0 is the incident energy (E_0 =200 keV), and β is the collection semiangle (β= 11 mrad). κ is the thermal conductivity of material, protein solution generally are worse conductors than pure water (κ_{water} = 0.58 W/m·K, $\kappa_{Si_3N_4}$ = 30.1 W/m·K, $\kappa_{protein}$ = 0.27 W/m·K).[4] x is the beam diameter (~1 μm in our experiments). T is the local temperature after heating, and T_0 is the surrounding temperature (298 K). R_0 is the conduction length, the distance from illuminating area to the bulk silicon (which with good conductivity of 149 W/m·K), is usually not longer than 500 μm. ε is the emissivity, and σ is the Stefan–Boltzmann constant (5.67×10^{-8} W/m^2·K^4). Here, the contribution of radiation heat transfer is almost ignorable. There are two very useful scripts for Digital Micrograph (TEM data process software, Gatan Inc.) written by D. R. G. Mitchell to do the above calculations quickly.[5]

Fig. S2(b) shows the calculated temperature rising (unit in K) from the above equations. Because of the good conductivity and thin thickness, the heating from electron collision on 100-nm silicon nitride (purple dash-dot line) is less than on 50-μm water (black solid line). Proteins usually are seemed as bad thermal conductors; KLH (blue short-dot line) presents a little higher temperature rising of 1−3 ℃ in the relative high beam current range of 5−10 nA. Under the operating parameters in our experiments (fluence rate of 10 to 3000 e$^-$/Å^2·s), the temperature rising from protein is lower than 0.003 K. Obviously, it is insufficient to give the minimum wall superheat (ΔT_{sat}) for nucleate boiling at a wall cavity in water; the homogeneous nucleation temperature is generally accepted as 303.7 ℃. When consider the effects of the contact angle (in the range from 50° to 110°), the dissolved air and the corner on the heterogeneous nucleation temperature of water (assume the critical nucleus radius r_c = 3.5 nm), the calculated necessary temperature is still over 180 ℃.[6] Even under an incredible-high electron beam

current of 200 nA, the temperature affected change of hydrogen solubility is ~0.5 % (ΔT = 60 °C) and almost ignorable (the solubility in water at 298 K and 358 K are 140.6 MPa·m^3/kmol and 141.4 MPa·m^3/kmol, respectively).[7] In summary, the electron-beam heating is not the cause of the nanobubbles appearance in our experiments.

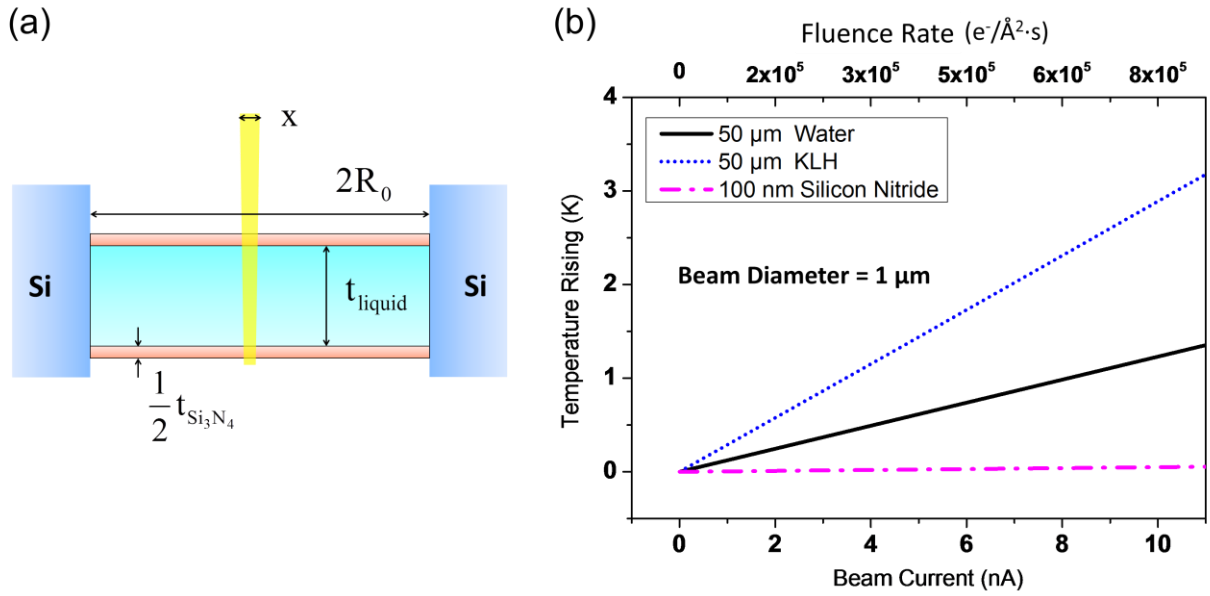

Fig. S2. Calculation of electron-beam heating. (a) Schematic illustration shows the dimensions for calculating. (b) A plot of calculated temperature rising from electron-beam heating on water (black solid line), KLH (blue short-dot line), and silicon nitride (purple dash-dot line).

Table S1. Calculated average energy loss and inelastic mean free path

Material	**Chemical Formula***	**Average Energy Loss**, $\langle E \rangle$ (eV)	**IMFP**, λ_i (nm)
Water	H_2O	11.72	188.4
KLH1	$C_{16187}H_{24168}N_{4400}O_{4684}S_{111}$	12.33	180.7
Silicon Nitride	Si_3N_4	17.41	135.9

* The atomic compositions of protein are calculated based on the sequences from ProtParam (a tool to compute the various physical and chemical parameters for a given protein)[8]. KLH1 (UniProt ID: Q6KC56)

Surface tension measurements of pure water and KLH solution

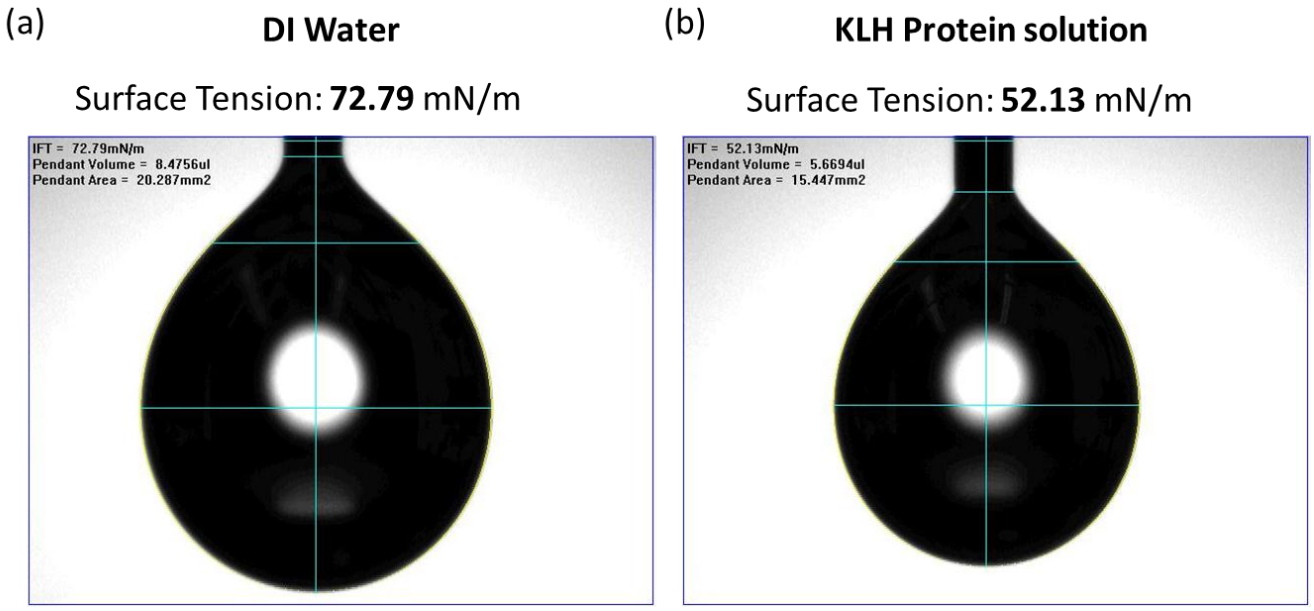

Fig. S3. Images of drop-shape analysis in pendant drop method interfacial tension measurements. (a) De-ionized water. (b) KLH solution (1 μM).

Calculation of theoretical hydrogen production rate *via* electron radiolysis

The production rate of hydrogen molecules from water radiolysis could be expressed by the format of product of hydrogen radiolytic yield (G_{H2}, so-called hydrogen G-value)[9] and the aborted electron dose rate (D_a/t), as shown in the following equations.

$$\left(\frac{dH_2}{dt}\right)_{Prod} = G_{H_2} \cdot \frac{D_a}{t} \qquad \text{(S5)}$$

The G_{H2} represents the number of molecules created or destroyed per 100 eV of energy deposited in the system. The theoritical maximium of G_{H2} in pure water radiolysis by beta (β) radiation is 0.53 molecules/100 eV.[9]

Absorbed dose, denoted D_a, represents the energy absorbed by matter in the unit and can be related to the product of incident electron flux (Φ, int the unit of $e^-/Å^2$) and the mass collision stopping power (S/ρ).[10] For 200 kV electron with flux of 10 $e^-/Å^2$, corresponding to a constant dose rate D_a/t is 44.76 M Gy/s (calculate from the collision stopping power of 2.793 MeV·cm^2/g estimated by NIST),[11] the conversed hydrogen production rate is about 96.3 fmole/s for a irradiated volume of 39.27 fL water.

'Goodness-of-fit' of the simple linear regression of bubble diameter against irradiation time

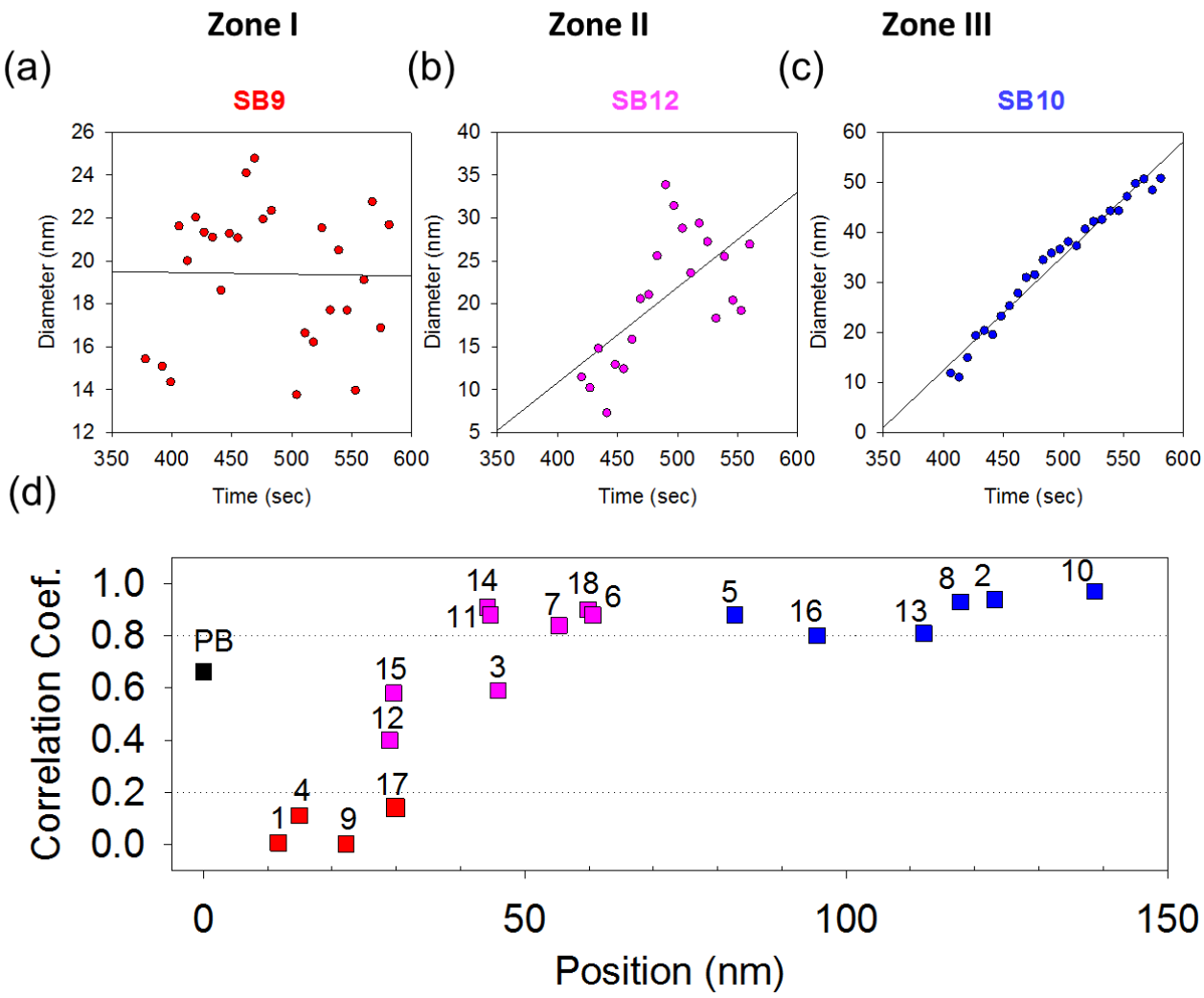

Fig. S4. Linear regression analysis of the bubble diameter against the total irradiation time. (a) A scatter plot shows a simple regression of the satellite NB (SB9) in zone I. (b) A scatter plot shows a simple regression of the satellite NB (SB12) in zone II. The SB12 has an oscillatory trajectory of growing diameters. (c) A scatter plot shows a simple regression of the satellite NB (SB10) in zone III. The SB10 has a linear trajectory of growing diameters. (d) A scatter plot of the coefficient of determination against the distance between primary NB and corresponding SB.

Supplementary Reference

(1) C. Gatsogiannis and J. Markl, *Journal of MolecularBbiology*, 2009, **385** (3), 963–983.

(2) R. F. Egerton, P. Li and M. Malac, *Micron*, 2004, **35** (6), 399–409.

(3) T. Malis, S. C. Cheng and R. F. Egerton, *Journal of Electron Microscopy Technique*, 1988, **8** (2), 193–200.

(4) A. Lervik, F. Bresme, S. Kjelstrup, D. Bedeaux and J. Miguel Rubi, *Physical Chemistry Chemical Physics*, 2010, **12** (7), 1610–1617.

(5) D. R. G. Mitchell and B. Schaffer, *Ultramicroscopy*, 2005, **103** (4), 319–332.

(6) J. Li and P. Cheng, *International Journal of Heat and Mass Transfer*, 2004, **47**, 2689–2698.

(7) U. J´auregui-Haza, E. J. Pardillo-Fontdevila, A. M. Wilhelm and H. Delmas, *Latin American Applied Research*, 2004, **34**, 71–74.

(8) M. R. Wilkins, E. Gasteiger, A. Bairoch, J. C. Sanchez, K. L. Williams, R. D. Appel and D. F. Hochstrasser, in *The Proteomics Protocols Handbook*; Humana Press, edited by John M.Walker, 2005; Vol. **112**, pp. 571–607.

(9) G. Merga, B. H. Milosavljevic and D. Meisel, *The Journal of Physical Chemistry B*, 2006, **110** (11), 5403–5408.

(10) T. Eriksen, in *Radiochemistry and Nuclear Chemistry*; Butterworth-Heinemann, edited by G. Choppin, J. Rydberg and J. O. Liljenzin, 2001; Chap. 7, pp. 166–191.

(11) M. Berger, J. Coursey, M. Zucker, and J. Chang, *NIST Stopping-Power and Range Tables for Electrons, Protons, and Helium Ions* [Online], December 9, 2011. http://www.nist.gov/pml/data/star/index.cfm (accessed September 17, 2012).